Bayesian Morphological Clock Methods Resurrect Placoderm Monophyly and Reveal Rapid Early Evolution in Jawed…

Article *in* Systematic Biology · December 2016

DOI: 10.1093/sysbio/syw107

CITATIONS
8

READS
456

5 authors, including:

Ben King
Flinders University
7 PUBLICATIONS **56** CITATIONS
SEE PROFILE

Tuo Qiao
Chinese Academy of Sciences
24 PUBLICATIONS **428** CITATIONS
SEE PROFILE

Min Zhu
Institute of Vertebrate Paleontology and Pale…
173 PUBLICATIONS **2,411** CITATIONS
SEE PROFILE

John Long
Flinders University
250 PUBLICATIONS **3,434** CITATIONS
SEE PROFILE

Syst. Biol. 0(0):1–18, 2016

DOI:10.1093/sysbio/syw107

Bayesian Morphological Clock Methods Resurrect Placoderm Monophyly and Reveal Rapid Early Evolution in Jawed Vertebrates

BENEDICT KING[1,*], TUO QIAO[2], MICHAEL S. Y. LEE[1,3], MIN ZHU[2], AND JOHN A. LONG[1]

[1]*School of Biological Sciences, Flinders University, PO Box 2100, Adelaide, South Australia 5001, Australia;* [2]*Key Laboratory of Vertebrate Evolution and Human Origins of Chinese Academy of Sciences, Institute of Vertebrate Paleontology and Paleoanthropology, Chinese Academy of Sciences, PO Box 643, Beijing 100044, China; and* [3]*Earth Sciences Section, South Australian Museum, North Terrace, Adelaide 5000, Australia*
**Correspondence to be sent to: School of Biological Sciences, Flinders University, PO Box 2100, Adelaide, South Australia 5001, Australia; E-mail: benedict.king@flinders.edu.au.*

Received 1 July 2016; reviews returned 4 September 2016; accepted 18 November 2016
Associate Editor: Thomas Near

Abstract.—The phylogeny of early gnathostomes provides an important framework for understanding one of the most significant evolutionary events, the origin and diversification of jawed vertebrates. A series of recent cladistic analyses have suggested that the placoderms, an extinct group of armoured fish, form a paraphyletic group basal to all other jawed vertebrates. We revised and expanded this morphological data set, most notably by sampling autapomorphies in a similar way to parsimony-informative traits, thus ensuring this data (unlike most existing morphological data sets) satisfied an important assumption of Bayesian tip-dated morphological clock approaches. We also found problems with characters supporting placoderm paraphyly, including character correlation and incorrect codings. Analysis of this data set reveals that paraphyly and monophyly of core placoderms (excluding maxillate forms) are essentially equally parsimonious. The two alternative topologies have different root positions for the jawed vertebrates but are otherwise similar. However, analysis using tip-dated clock methods reveals strong support for placoderm monophyly, due to this analysis favoring trees with more balanced rates of evolution. Furthermore, enforcing placoderm paraphyly results in higher levels and unusual patterns of rate heterogeneity among branches, similar to that generated from simulated trees reconstructed with incorrect root positions. These simulations also show that Bayesian tip-dated clock methods outperform parsimony when the outgroup is largely uninformative (e.g., due to inapplicable characters), as might be the case here. The analysis also reveals that gnathostomes underwent a rapid burst of evolution during the Silurian period which declined during the Early Devonian. This rapid evolution during a period with few articulated fossils might partly explain the difficulty in ascertaining the root position of jawed vertebrates. [Bayesian; BEAST; morphological clock; morphology; monophyly; phylogenetics; placoderms; tip dating; tree topology.]

The phylogeny of early vertebrates is vital for understanding the acquisition of key characters at the origin of gnathostomes. Jawed vertebrates, today comprising the bony fish (osteichthyans) and the cartilaginous sharks and rays (chondrichthyans), contain over 99% of living vertebrate diversity, and share derived features including jaws, teeth, paired fins, paired nasal capsules and three semicircular canals that are absent in living jawless vertebrates. Key to the early evolution of jawed vertebrates is the placoderms, a group of armoured fishes that dominated vertebrate faunas until their extinction at the end of the Devonian period (ca. 359 Ma). Early treatments of placoderm relationships considered them to be a paraphyletic group, giving rise independently various groups of elasmobranchs (Ørvig 1962; Stensiö 1963, 1969). This hypothesis was later rejected and placoderm monophyly was advocated (Goujet 1982, 1984b, 2001). Placoderm monophyly was challenged by a study on the vascularization of the pectoral fin of antiarchs (Johanson 2002), but this was disputed (Young 2008). Placoderms have been hypothesized to be the sister group to chondrichthyans (Miles and Young 1977; Janvier 1996), or osteichthyans (Forey 1980; Gardiner 1984a), but are more often considered sister to other gnathostomes (Schaeffer 1975; Young 1986; Goujet 2001; Goujet and Young 2004). The first cladistic studies that explicitly tested placoderm monophyly rejected it in favor of a phylogenetic hypothesis in which placoderms were a paraphyletic assemblage of stem gnathostomes (Friedman 2007; Brazeau 2009). Although placoderms share many features not found in other gnathostome groups (Young 2010), these characters are contentious as, among other problems, many cannot be polarized by outgroup comparison (Brazeau 2009; Brazeau and Friedman 2014).

The current view of placoderm paraphyly implies that features common to placoderms are primitive for all gnathostomes. This has important implications for the study of key morphological features including teeth (Smith and Johanson 2003; Rücklin et al. (2012)), braincase morphology (Dupret et al. 2014), the skull and jawbones (Zhu et al. 2013), and internal fertilization (Long et al. 2015). However, support for placoderm paraphyly is acknowledged to be weak (Brazeau and Friedman 2015). The discovery that dermal claspers and therefore internal fertilization is apparently widespread across placoderm groups (Miles and Young 1977; Long et al. 2015; Trinajstic et al. 2015) also weakens support for placoderm paraphyly as it requires a reversal to external fertilization at the crown gnathostome node (Brazeau and Friedman 2015). There is little or no evidence of a reversal from internal to external fertilization, or from viviparity to oviparity, occurring in any recent group of fishes (Blackburn 2015), despite multiple origins, and it is possible that internal fertilization

is an irreversible or nearly irreversible character. The uncertainty in phylogenetic relationships at the base of the gnathostomes is potentially driven by outgroups with morphologies that are difficult to compare with gnathostomes, or lack detailed neurocranial preservation.

The recent application of relaxed clock Bayesian methods to morphological paleontological data (Lee et al. 2014; Close et al. 2015; Gavryushkina et al. 2015) provides the opportunity to gain a more complete picture of the evolution of extinct groups. Here, this method is applied to an expanded early gnathostome data set. Although character support for either placoderm monophyly or paraphyly is essentially equivocal, the tip-dated, morphological clock method finds strong support for placoderm monophyly, suggesting that this approach can have effects on tree topology as well as analysing rates of evolution. Observed and simulated patterns of rate heterogeneity provide tentative evidence that the result from the tip-dated clock analysis may be the correct one. The possibility of a very different topology in early gnathostome phylogeny—in which placoderms are monophyletic and thus not necessarily representative of the plesiomorphic gnathostome condition—must be considered when studying early vertebrate evolution. Throughout this paper, we use the term placoderms to refer to the core group, excluding the maxillate placoderms such as *Entelognathus*. It is monophyly of this core group that is strongly supported by Bayesian tip-dated clock methods.

Materials and Methods

Data Matrix

Characters were drawn from previous analyses on early gnathostomes (Brazeau 2009; Davis et al. 2012; Zhu et al. 2013; Dupret et al. 2014; Brazeau de Winter 2015; Giles et al. 2015; Long et al. 2015), from a number of other sources (Coates and Sequeira 2001; Friedman 2007; Zhu and Gai 2007; Dupret et al. 2009; Sansom 2009; Swartz 2009; Trinajstic and Long 2009; Carr and Hlavin 2010; Jia et al. 2010; Pradel et al. 2011; Lu et al. 2012; Pan et al. 2015; Zhu et al. 2015), as well as newly formulated characters.

To ensure the data set satisfied the assumptions of tip-dated, morphological clock analysis, we attempted to sample characters with equal intensity across the whole phylogeny including terminal branches (undersampled in the majority of published morphological data matrices). We therefore included autapomorphies (character states found in only one sampled taxon), and characters applicable only to small subsets of taxa. We imported some autapomorphies from matrices of subclades in which they were phylogenetically informative due to denser taxon sampling. Others were new and selected if they constituted morphological variation qualitatively similar to the phylogenetically informative characters. We recoded terminal taxa at the species level, and reformulated the outgroup as constituent species rather than superspecific taxa. Galeaspid histological characters are best known from isolated fragments (Wang et al. 2005). We included these as a separate taxon, and constrained a group consisting of this purely histological taxon (polybranchiaspid sp. histological samples) and two polybranchiaspid species to be monophyletic in all analyses.

The matrix had a total of 117 taxa and 497 characters. The full list of characters, characters sources, taxa and taxon sources are in the Supplementary Information, available on Dryad at http://dx.doi.org/10.5061/dryad.v30f1. New and revised characters are in bold. The matrix was assembled in Mesquite 3.04 (Maddison and Maddison 2015) and the nexus file is included in the Dryad repository.

Parsimony Analysis

We performed parsimony analysis in TNT (Goloboff et al. 2008), using a traditional search strategy with 5000 random addition sequence replicates, saving 10 trees in each replicate. Due to the extremely large number of shortest trees we did not perform a fully exhaustive tree search. 6490 shortest trees of length 1175 were collected. We ran an additional analysis with a negative (=reverse) constraint on placoderm monophyly (i.e., to find the shortest tree in which placoderms were not monophyletic), resulting in 5950 trees of length 1176. One of the shortest trees from each analysis was loaded into PAUP* 4.0b10 (Swofford 2002) to extract lists of characters that differed in length between the two topologies.

Tip-Dated Morphological Clock Analysis

We used BEAST2.3.2 (Bouckaert et al. 2014) for tip-dated morphological clock analyses via Bayesian MCMC. We assembled Xml files manually, using output from both BEAUti2.3.2 and BEASTmasteR (Matzke 2015).

We used a sampled-ancestor fossilized birth death tree prior (Gavryushkina et al. 2014). Due to the absence of extant taxa, we did not implement a rho parameter. We fixed removal probability at 0 as this describes an epidemiological process not applicable to fossils.

Recently there has been a trend toward partitioning morphological analyses by the number of states (Close et al. 2015; Gavryushkina et al. 2015), as opposed to using a single partition with the number of states equal to the maximum number observed in the matrix (Lee et al. 2014). The partitioned model typically has a far superior marginal likelihood (~1000 log likelihood units in this case). The partitioned model, however, has the unintended side-effect of upweighting changes in multistate characters. This is due to the lower stationary frequencies in partitions with higher numbers of states. There is no clear biological justification for the effective upweighting of changes in characters with high number

of states. Splitting characters into more states already artificially upweights them by increasing the number of changes, so it could be argued that each change in such characters should be, if anything, downweighted. Compounding this problem by using a typical existing partitioned model is undesirable. The solution employed here is to partition the data set by number of states (one partition for two state characters and one for three state characters), but to increase the exchangeability values (mutationRate in the xml files) in the partition with three state characters. Increasing the exchangeability values to 1.5 for three state characters, 2 for four states, etc. exactly counteracts effect of the lower stationary frequencies. This model will be referred to as the partitioned reweighted model. Two partitions were used as the data matrix only had characters with two or three states.

We tested different partitioning schemes and clock models using path sampling (Baele et al. 2012). After a burn-in of 30,000,000 generations, we ran path sampling analyses for 30 steps, each of 10,000,000 generations. Alpha was 0.3 and each step had an additional burn-in period of 10%. We tested three different partitioning schemes: unpartitioned, partitioned, and partitioned reweighted (see above). We tested a strict clock against the lognormal uncorrelated relaxed clock (Drummond et al. 2006). Finally, we tested models with and without a gamma parameter with four discrete rate categories to account for rate variation across sites. The prior distributions for each parameter are detailed in the Supplementary Information, available on Dryad.

We performed a number of sensitivity analyses to test the robustness of conclusions to various model assumption violations. One analysis excluded all taxa occurring after the Frasnian. This eliminates the large number of stratigraphically late chondrichthyans which were originally included to compensate for a depauperate Devonian record. However, the lack of sampling of non-chondrichthyan taxa in this time period may bias the tree prior model which assumes equal sampling across the phylogeny. A second sensitivity analysis tested the effect of the stratigraphic uncertainty, that is, the specified tip dates. We ran an analysis where 28 taxa with relatively large dating uncertainty (>c.5 Myr) were given uniform age range priors over the period of uncertainty (see Supplementary Information, available on Dryad, for the age ranges used). Because the sampling process in this analysis can allocate separate ages to fossils found in the same site (and thus with the same age ranges), we used this analysis simply to test sensitivity to the tip date uncertainty.

We ran analyses for four independent runs of 200,000,000 generations each. Some analyses were run on the CIPRES Science Gateway (Miller et al. 2010). Convergence was assessed by superimposition of parameter traces of all four runs in Tracer (Rambaut et al. 2014) and ESS > 200 for all parameters. Post burn-in samples from the four runs were combined for further analysis and figures. The maximum clade consensus tree was calculated. Because of the significant phylogenetic uncertainty at the root of the ingroup (gnathostomes) found in the Bayesian clock analysis, we wrote an R function that returns the posterior probability of multiple clades being monophyletic (simultaneously) in the posterior sample of trees. This function was dependent on packages ape (Paradis et al. 2004) and caper (Orme et al. 2013). The function included the option to prune rogue taxa from all trees prior to analysis. For the credible set of topologies shown in Figure 4b, the unstable taxon *Ramirosuarezia* (Pradel et al. 2009) was dropped from all trees, and all probabilities assume that osteichthyans, placoderms, and acanthodians/chondrichthyans are monophyletic. R code for this function (monophy.multi.R) is in the Dryad repository.

To examine how rates of evolution vary through time, the data set was analysed in BEAST1.8.3 (Drummond et al. 2012), which implements an epoch clock (Bielejec et al. 2014), that assigns a separate evolutionary rate to specified time slices. As for the BEAST2 analysis, a partitioned model with reweighted three-state characters was implemented. The tree prior was a birth–death serial sampled model (Stadler 2010). Seven time slices were specified. The first was pre-Silurian with no upper bound, followed by the Silurian, Lochkovian/Pragian, Emsian, Middle Devonian, Late Devonian, and Carboniferous. The epoch clock analysis was run for 100,000,000 generations (four independent runs) and convergence checked as above.

Because the epoch clock applies strict clock rates to each time slice, it may not be a realistic model when there is rate variation within time slices (e.g., across lineages). To see if the same patterns found in the epoch clock analysis held in the relaxed clock analysis (which allowed rates to vary across lineages), a function in R was written to extract weighted mean rates in each time slice across the posterior sample of trees and plot them against the geological timescale. The packages OutbreakTools (Jombart et al. 2014), picante (Kembel et al. 2010), and geoscale (Bell 2015) were required. The R code for these functions (get.epoch.rates and geoplot.epoch.rates) is in the Dryad repository.

Simulations: Testing the Performance of Different Methods in Rooting Phylogenetic Trees in the Absence of Informative Outgroups

Since very different root positions for the ingroup gnathostome clade were retrieved from the parsimony and Bayesian clock methods, simulations were performed to investigate the performance of these methods. Simulations were performed in BEAST2.3.2, using models and parameters based on the results from BEAST. Simulations were based on two trees taken from preliminary runs of the gnathostomes data set in BEAST. The first was an unconstrained tree representing a relatively balanced phylogeny (i.e., with placoderms monophyletic). The second was from a constrained run with placoderms paraphyletic, representing a relatively unbalanced phylogeny. 500 two-state characters were

simulated using values similar to empirical values: a lognormal-relaxed clock with mean rate 0.08 and a gamma parameter with alpha 2 to represent among-character rate variation; the standard deviation of the clock lognormal distribution was 0.9 for the balanced tree and 1.0 for the unbalanced tree. Twelve simulation replicates on each tree were performed. 73% of the simulated data were removed from the outgroup (reflecting the empirical situation here where only 27% of characters are scorable to both the outgroup and the ingroup, a likely cause for instability in the root position). The simulated data were reanalysed in TNT using 1000 random addition sequence replicates saving 10 trees in each replicate, and strict and 50% majority rule consensus trees were calculated. Reanalysis in BEAST used the same model parameters and priors as the analysis on the empirical data set, with the exception of a wide uniform prior on mean clock rate (0–1000). The correct clock model and tip ages were assumed. Analyses were run for 200,000,000 generations and convergence checked as for other BEAST analyses.

Revisions to Characters Supporting Placoderm Paraphyly

Position of the Hyoid Arch and Orientation of the Hyomandibular Nerve

Evidence for placoderm paraphyly in previous analyses may have been inflated due to inclusion of multiple characters associated with the same morphological feature: the anterior position of the jaws in some placoderms, and the anterior position of the gill arches in osteostracans (an agnathan outgroup). The following characters have supported paraphyly with state 1 uniting a subset of placoderms (especially arthrodires) and crown gnathostomes:

1. Position of hyomandibula articulation on the neurocranium: 0) below or anterior to orbit, on ventrolateral angle of braincase; 1) on otic capsule, posterior to orbit. Brazeau (2009) character 89; Davis et al. (2012) character 95; Zhu et al. (2013) character 95; Dupret et al. (2014) character 95; Long et al. (2015) character 95; Giles et al. (2015) character 163.

2. The main trunk of facial nerve (N.VII): elongate and passes anterolaterally through orbital floor; 1) stout, divides within otic capsule at the level of the transverse otic wall. Brazeau (2009) character 71; Davis et al. (2012) character 69; Zhu et al. (2013) character 69; Dupret et al. (2014) character 69; Long et al. (2015) character 69; Giles et al. (2015) character 137.

3. Position of upper mandibular arch cartilage (and associated cheek plate where present): 0) entirely suborbital; 1) with a postorbital extension. Giles et al. (2015) character 95.

4. Orbit dorsal or facing dorsolaterally, surrounded laterally by endocranium: 0) present; 1) absent. Brazeau (2009) character 68; Davis et al. (2012) character 66; Zhu et al. (2013) character 66; Dupret et al. (2014) character 66; Long et al. (2015) character 66; Giles et al. (2015) character 130.

*The hyomandibular articulation and the hyomandibular nerve (*Fig. 1*).*—The hyomandibular nerve character is problematic for two reasons. Firstly, it is not clear that characters involving the division of the hyomandibular nerve can be applied to agnathans. The hyomandibular nerve of lampreys does not appear to have any pretrematic or palatine branches (Johnston 1905; Kuratani et al. 1997), and this appears to also be the case in osteostracans (Stensiö 1927). Therefore, the division of the hyomandibular nerve mentioned by Brazeau and Friedman (2014) may not be equivalent to a palatine ramus. However, a character concerning only the orientation of the nerve may still be useful, but this is not independent from the position of the hyomandibular articulation. The hyomandibular nerve will necessarily go through the orbit when the hyoid arch is positioned anteriorly. The character concerning the nerve is therefore redundant and can be deleted in favor of the character concerning the attachment of the hyoid arch, which can be scored in more taxa. In addition, this character is variable within the outgroup. The hyoid arch in galeaspids is posterior to the orbits (Fig. 1e), and if it is scored as such then both placoderm monophyly and paraphyly are equally parsimonious for this character.

The upper mandibular arch.—This character was only included by Giles et al. (2015). It refers to the suborbital position of the "upper mandibular arch cartilage" which was scored as "entirely suborbital" in the outgroups and some placoderms. However, it is questionable whether or not this character should be scored in the outgroups. Mandibular arch derivatives occupy an extensive domain in living agnathans, as opposed to gnathostomes in which they are confined to a distinct domain between the premandibular and hyoid regions (Miyashita 2015). The mandibular arch cartilages of living agnathans (the velar and lingual cartilages) are not exclusively suborbital, and it is not clear that one or the other can be homologized with the palatoquadrate in a straightforward manner. As far as can be assessed, conditions in the osteostracans and galeaspids are more similar to extant agnathans than gnathostomes (Janvier 1996; Miyashita 2015). This character should be inapplicable in outgroups. Within gnathostomes, this character is not independent from the character concerning the position of the hyomandibula articulation, as the mandibular and hyoid arches are expected to move forwards in tandem given the supporting role of the latter for the former. This character is deleted here due to redundancy, but it should not affect placoderm paraphyly/monophyly if correctly scored.

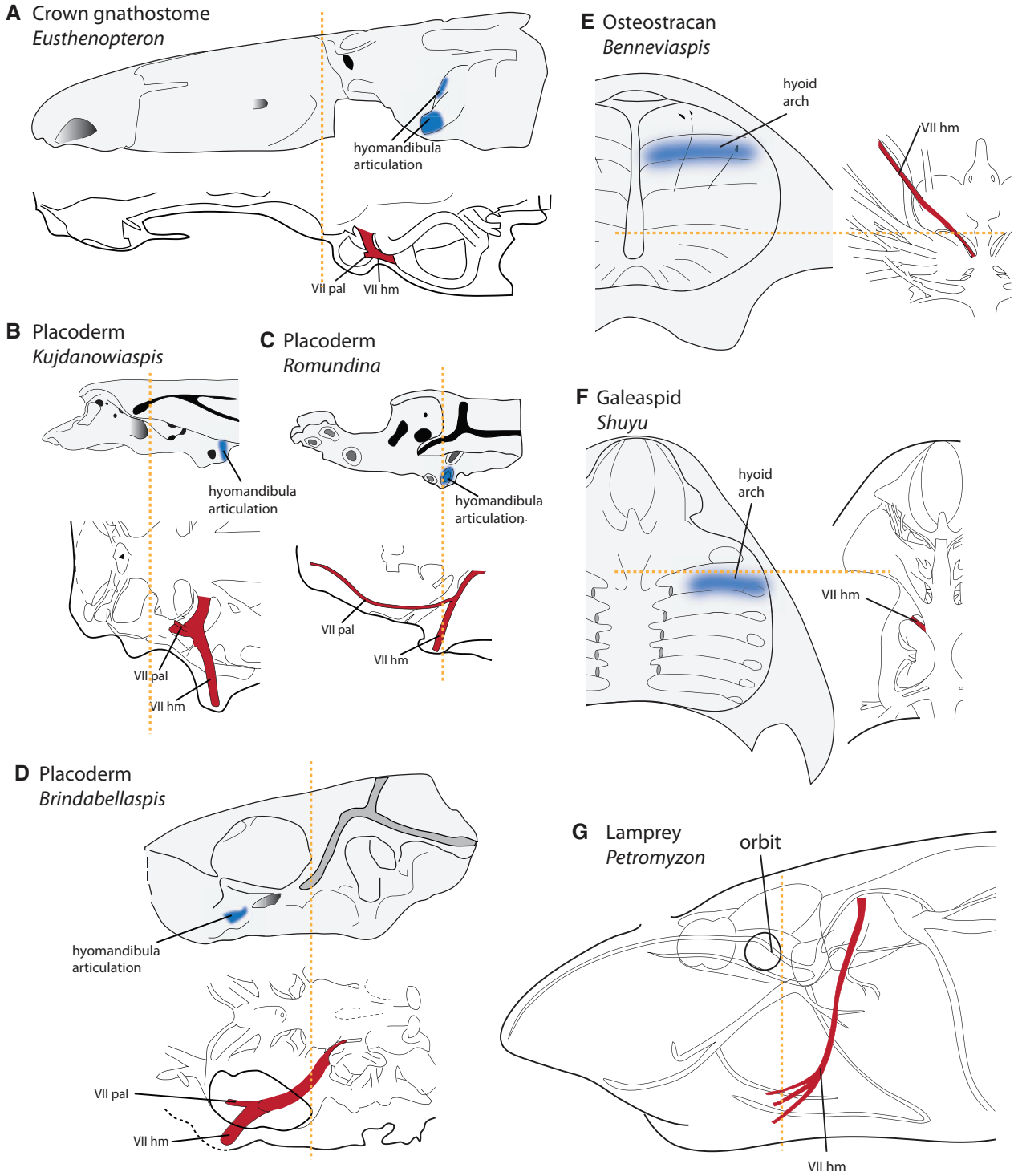

FIGURE 1. Characters that supported placoderm paraphyly, concerning the position of the hyoid arch and the orientation of the facial nerve, are correlated—and variable in the jawless outgroups. **a**–**d**) Gnathostomes, external view of braincase in left lateral view and dorsal view of braincase showing outline of the cranial cavity and nerves (b is in ventral view). Dotted lines mark posterior of the orbits. The hyoid arch articulation character is effectively continuous, ranging from an articulation posterior to the orbits (a–b), to suborbital (d) or intermediate (c). The orientation of the hyomandibular nerve and the position of the division of the palatine nerve are correlated with the hyomandibular articulation position. **e**–**f**) Agnathans, braincase in ventral view and ventral view showing outline of cranial cavity and nerves. **g**) Lamprey in left lateral view showing outline of cranial nerves. The anterior position of the hyoid arch and facial nerve in osteostracans (e) is not found in other agnathan groups (f–g). Characters based on the division of facial nerve are inapplicable in agnathans (g) as they do not have a palatine nerve. Sources: a) Jarvik (1980); b) Dupret (2010) and Goujet (1984a); c) Dupret et al. (2014); d) Young (1980); e) Janvier (1985); f) Gai et al. (2011); g) Johnston (1905).

Orbit surrounded by endocranium.—The orbit being surrounded by endocranium may also be linked to the anterior migration of the hyomandibular attachment. In most placoderms, the hyomandibula attaches to the anterior postorbital process, but when the hyomandibula attaches in an anterior position this part of the braincase must also extend forward to provide a surface for attachment. In *Romundina*, *Macropetalichthys*, and *Brindabellaspis* successively further anterior hyomandibular attachments lead to a greater proportion of the orbit being surrounded by neurocranium. However, because the condition in *Doliodus* demonstrates that this character is at least partly independent from the position of the hyomandibular attachment, this character has been retained in all analyses.

When this character complex is reduced to a simple character involving the position of the hyoid arch relative to the orbits, it can be seen to be effectively continuous (Fig. 1a–d), with the posterior of the orbit used to split the character into two states. Jawless vertebrates show similar variation in the positions of the gill arches relative to the orbits (Fig. 1e–g), with an extreme anterior position being a feature of osteostracans. Independent acquisition of an anterior hyoid arch in some placoderms and osteostracans (consistent with placoderm monophyly) is therefore equally parsimonious with a single acquisition and secondary loss (consistent with placoderm paraphyly).

Trigemino–Facial Recess

Presence of a trigemino–facial recess, as scored in Giles et al. (2015) is an important character as it unites rhenanid placoderms with crown gnathostomes, thus supporting placoderm paraphyly. The character was introduced by Davis et al. (2012), citing Goodrich (1930), Schaeffer (1971), Gardiner (1984b), and Maisey (2005) as sources. These references give differing definitions however, and none would support a shared condition in rhenanids and crown gnathostomes.

Goodrich (1930), following Allis, described the trigemino–facial chamber as consisting of two parts. The first is the pars ganglionaris, a "recess" of the cranial cavity (i.e., an outpocket) containing the trigeminal and facial ganglia. The second is the pars jugularis, a space between the lateral commissure and the lateral cranial wall through which the jugular vein passes. These form a divided chamber when the lateral endocranial wall is complete (prefacial commissure), and an undivided chamber when this is broken down such that the pars ganglionaris and pars jugularis are confluent. Goodrich defined the trigemino–facial recess as only the divided condition.

Schaeffer (1971) on the other hand argued against the definition of using a single term for a divided chamber, when the division was such a fundamental feature as the endocranial wall. Schaeffer's definition restricted the term trigemino–facial recess to the space between the lateral cranial wall and the lateral commissure. Under this definition the actual position of the trigeminal and facial ganglion becomes irrelevant (Schaeffer 1971). Gardiner (1984b) followed this definition and noted that it could also apply to chondrichthyans. This definition of the trigemino–facial recess is also not useful here, as the lateral commissure and jugular canal are already dealt with in other characters. Also, in sarcopterygians such as *Eusthenopteron*, the lateral commissure is offset posteriorly from the trigeminal and facial nerves.

The rhenanid *Jagorina* is depicted as having a large trigemino–facial–acoustico recess in Stensiö (1969). This is an intramural recess of the cranial cavity, which might correspond to the pars ganglionaris of Goodrich (1930). It is not a trigemino–facial chamber under the definition formed by Schaeffer (1971) for the trigemino–facial chamber. Schaeffer in fact apparently had different definitions for the trigemino–facial chamber and the trigemino–facial recess, the latter referring to the intramural recess.

Thus, the condition in rhenanids corresponds to the trigemino–facial recess of Schaeffer, but not the trigemino–facal chamber. Davis et al. (2012) however refer to their trigemino–facial recess as extra-mural, and therefore appear to be referring to the chamber rather than the recess of Schaeffer. This cannot match the condition in rhenanids.

Maisey (2005) discussed the acoustico–trigemino–facial recess, an internal space containing the roots of the trigeminal, facial, and acoustic nerves. Also discussed is the trigeminal pituitary fossa, which contains the pituitary vein, abducens nerve, external rectus muscle, and the ganglia for the trigeminal and facial nerves in neoselachians. This fossa does not house the trigeminal or facial ganglia in *Cladodoides* and on this basis, a trigemino–facial recess was determined to be absent in *Cladodoides* (Maisey 2005). In the placoderm *Brindabellaspis*, the trigeminal and facial nerves open into the myodome for the external rectus muscle, and so a trigemino–facial recess could be said to be present (Gardiner 1984b; Maisey 2005).

If an expanded definition of a trigemino–facial recess is used, based on one of these references is used, possibilities for how they would be scored are as follows:

1. Goodrich (1930). A continuous space between the lateral commissure and the cranial cavity formed by the breakdown of the wall between the pars ganglionaris and the pars jugularis. Originally described in *Amia* and other basal actinopterygians; could be said to be present in *Acanthodes*.

2. Schaeffer (1971). The space between the lateral commissure and the lateral cranial wall. This character would not be independent of other characters concerning endocranial processes and the jugular vein, and the position of the trigeminal and facial nerves would be irrelevant.

3. Maisey (2005). A fossa containing the abducens nerve, external rectus muscle, pituitary vein, and the trigeminal nerve. This would be present in some chondrichthyans and *Brindabellaspis*.

While the trigeminal and facial nerves and their respective ganglia are no doubt a source of useful characters, no condition clearly links rhenanids and crown gnathostomes. In the current matrix, this character is deleted, but reinstatement in modified form at a later date is likely.

Results

Parsimony

Parsimony analysis showed that placoderm paraphyly and monophyly are essentially equally parsimonious. The strict consensus tree has placoderms monophyletic, but placoderm paraphyly is a single step longer (Fig. 2). The two topologies are essentially identical apart from the root position within the ingroup clade (gnathostomes). The first topology places the gnathostome root between placoderms and all other gnathostomes, resulting in reciprocal monophyly; the second topology places the root within placoderms, thus rendering placoderms paraphyletic with respect to crown gnathostomes. Characters that differ in length between the two topologies are shown in Table 1.

Bayesian Morphological Clock Analysis

Stepping stone analysis supported partitioning of characters by the number of observed character states (marginal log likelihood −5601.52) over an unpartitioned model (−6601.78). There was a further increase in support for the model in which the substitution rates in the three-state partition were increased (to 1.5) to compensate for the lower stationary frequencies (marginal log likelihood −5589.64). The uncorrelated lognormal relaxed clock was supported over the strict clock (marginal log likelihood −5671.86) and use of a gamma parameter to describe among-character rate variation was preferred over a model with no such rate variation (marginal log likelihood −5646.95), with the latter two tests implemented under the partitioned reweighted model.

The tip-dated morphological clock analysis in BEAST strongly supports placoderm monophyly (Fig. 3), with a posterior probability of 0.997. Only 6 of the 7204 sampled trees correspond to a phylogeny consistent with placoderm paraphyly, in which antiarchs and acanthothoracids are sister group to other gnathostomes (pp = 0.0008).

Many of the basal nodes in the phylogeny are however very weakly supported (Figs. 3 and 4). Although the monophyly of placoderms, osteichthyans, and the acanthodian–chondrichthyan clade receives strong posterior probabilities, their relationships to each other and to *Entelognathus* and *Janusiscus* are unresolved. This topological uncertainty is graphically demonstrated in the program DensiTree (Bouckaert 2010), which plots all trees in the posterior sample on top of each other. The DensiTree plot (Fig. 4a) shows complex webs at the base of the gnathostomes, among the placoderm orders, and among acanthodians. Relationships among osteichthyans generally appear more robust, with the exception of *Guiyu*, *Achoania*, and *Psarolepis*, which appear to be flipping between various positions at the base of the osteichthyans. The instability at the gnathostome root means that the consensus tree (Fig. 3) does not represent a complete picture of the results. Ten different topologies representing different relationships among placoderms, osteichthyans, acanthodians/chondrichthyans, *Entelognathus*, and *Janusiscus* account for 85% of the posterior density (*Ramirosuarezia* was pruned from all trees prior to calculation of posterior probabilities). Almost every possible topology concerning these five taxa is sampled at appreciable frequency. This is despite many of these topologies contradicting a large amount of cladistic morphological evidence, that is, they are up to 16 steps longer under parsimony (Fig. 4b). Apparently, the morphological clock analysis can accommodate a substantial amount of homoplasy on temporally long basal branches without significant penalty. It is perhaps notable that despite this exaggerated uncertainty near the root, placoderm paraphyly is virtually never sampled.

It is possible that the uncertainty near the root is being driven by the exceptionally fast rates on the branches leading to osteichthyans and acanthodians/chondrichthyans. A branch with outlier rate may not fit the clock model well. Placing the gnathostome root on this branch effectively divides it into two branches, potentially with reduced rates. An analysis with artificially lowered rates on these branches (through character deletion) was used to test this, but a similar degree of uncertainty at the root was still found (not shown). Thus, sampling of unparsimonious topologies near the gnathostome root does not appear to be an artifact of fast-evolving branches.

Effect of Character Revisions on the Outcome of Analyses

To test the effect of the character revisions in the previous section on the outcome of the analyses we analyzed a data set with these characters (division of facial nerve, position of upper mandibular arch cartilage, trigemino–facial recess) reinstated. This included (what we regard as) incorrect codings that would lead these characters to support placoderm paraphyly (see above). The tip-dated morphological clock analysis still strongly supports placoderm monophyly (pp = 0.962). This shows that consideration of stratigraphic ages and as well as rates of evolution can override weak cladistic signals regarding tree topology.

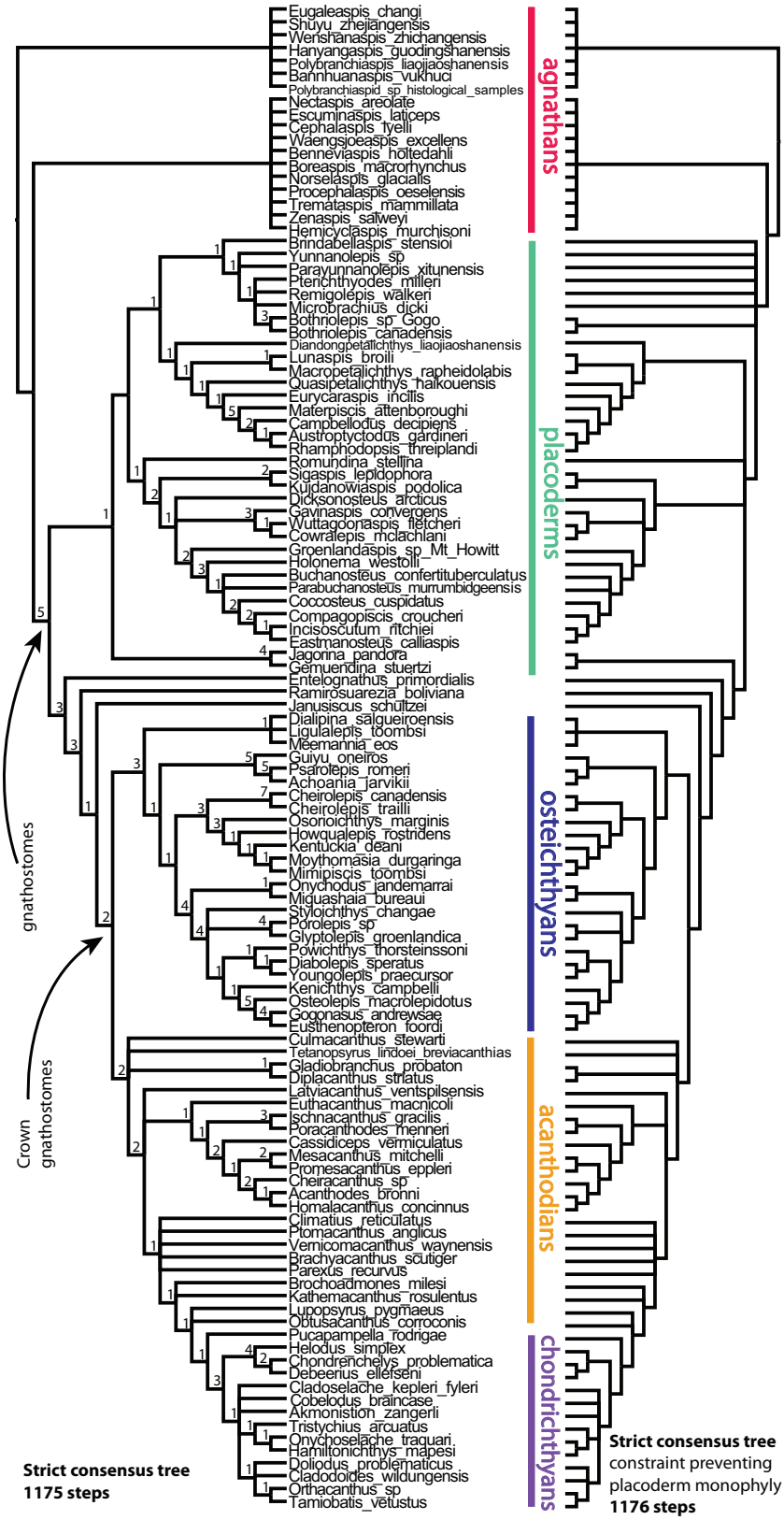

FIGURE 2. Results of parsimony analysis of the revised gnathostomes data set show placoderm monophyly and paraphyly are essentially equally parsimonious. Left: Strict consensus tree of unconstrained analysis. Right: Strict consensus tree of an analysis with negative constraint on placoderm monophyly. Numbers on the left tree refer to Bremer support values.

TABLE 1. Characters that differ in length between trees in which placoderms are paraphyletic and monophyletic

Character	Number of steps when placoderms are paraphyletic	Number of steps when placoderms are monophyletic
20. Nasal openings: 0) dorsal, placed between orbits, 1) ventral and anterior to orbits	**2**	3
30. Orbit dorsal or facing dorsolaterally, surrounded laterally by endocranium: 0) absent; 1) present	**3**	4
73. Optic fissure: 0) present; 1) absent	2	**1**
76. Jugular canal: 0) long; 1) short; 2) absent	**3**	4
87. Paired occipital facets	2	**1**
208. Dermal plate associated with pineal eminence or foramen: 0)contributes to orbital margin; 1) separated from orbital margin	**1**	2
395. Intromittent organ not associated with pelvic fins	2	**1**
465. Synarcual	3	**2**
468. Longitudinal scale alignment in fin webs	4	**3**

Note: Bold denotes which topology is favored (fewer character changes)

Rates of Evolution in Early Vertebrates

The epoch clock analysis in BEAST1.8.3 shows a broad picture of declining rates following an initial burst during the early period of gnathostome evolution (Fig. 5a). The earliest time bin (prior to the Silurian) has a very wide posterior distribution, as expected due to the small number of branches. The last two time bins (Late Devonian and Carboniferous) are unlikely to be meaningful due to poor sampling of non-chondrichthyan taxa. The other four time bins (Silurian, Lochkovian-Pragian, Emsian, Middle Devonian) should therefore form the basis of comparison. The posterior distributions of the rate estimates do not overlap between the Silurian and the Emsian and Middle Devonian, whereas the Lochkovian–Pragian rates are intermediate. The mean posterior estimates for the evolutionary rate during these time slices are 0.00670, 0.00496, 0.00204, and 0.00272, suggesting that rates of evolution were approximately three times greater during the Silurian than the latter part of the Devonian.

The weighted mean rate estimates over the same time slices from the posterior sample of trees constructed using the uncorrelated lognormal relaxed clock in BEAST2.3.2 shows a similar pattern of declining rates (Fig. 5b), although the overall differences between epochs are slightly less substantial. The mean posterior estimates for weighted mean rate in the Silurian, Lochkovian–Pragian, Emsian, and Middle Devonian are 0.00558, 0.00487, 0.00360, and 0.00358. Therefore, during the Silurian, rates were only about 50% higher than during the latter part of the Devonian according to the relaxed clock. The higher rate estimates in the Silurian are inferred despite a total absence of any internal node or root age constraints. When a maximum age of 440 Ma is applied to the gnathostome node, rates in these time slices become 0.00917, 0.00608, 0.00390, and 0.00407, more in line with the results from the epoch clock although the increase in rates across all time slices is intriguing. The pattern of declining rates appears to be robust, and also present in the sensitivity analyses (Supplementary Figs. S1–S3, available on Dryad). Analyses with constrained placoderm paraphyly, no post-Frasnian taxa or variable tip dates show the same pattern.

In terms of rates on individual branches, the relaxed clock analysis shows exceptionally high rates of evolution at the base of the osteichthyans and the acanthodian–chondrichthyan clade (Fig. 3). No such burst is present at the origin of placoderms.

Performance of Different Methods in Simulations

To test the performance of parsimony and the tip-dated morphological clock analysis in rooting the ingroup, simulations of 500-character data sets, with 73% of data removed from the outgroup (discussed above) were performed. Simulations (12 replicates on each tree) were performed on two trees, the first was a relatively balanced tree taken from a preliminary BEAST analysis, corresponding to the situation in which placoderms are monophyletic. The second was a relatively unbalanced tree, corresponding to placoderm paraphyly. Results of the simulations are shown in Table 2. Numbers indicate

TABLE 2. Results from simulations

Tree 1			Simulation number	Tree 2		
Parsimony	BEAST	Posterior probability		Parsimony	BEAST	Posterior probability
9	**0**	**0.708**	1	6	6	0.000
0	0	0.989	2	2*	1	0.241
Polytomy	0	0.419	3	**5**	**1**	**0.184**
2	1	0.527	4	1	2	0.103
0	0	0.499	5	**9**	**1**	**0.151**
1	0	0.869	6	**5**	**2**	**0.013**
0	1	0.409	7	4	4	0.061
1	1	0.227	8	**8***	**2**	**0.042**
0	0	0.998	9	**4***	**2**	**0.058**
0*	1	0.191	10	0	1	0.385
2	1	0.516	11	1*	2	0.082
0	0	0.398	12	4	3	0.442

Notes: Two trees were used for the simulations, tree 1 similar to the consensus tree from BEAST (a balanced tree with corresponding to placoderm monophyly) and tree 2 an unbalanced tree corresponding to placoderm paraphyly. 73% of data in the outgroup were removed prior to reanalysis in BEAST and parsimony. Numbers refer to the number of nodes between the root found in the consensus tree and the correct root (i.e., lower is better and 0 means the correct root was found). For parsimony a strict consensus tree was used, but where this resulted in an uninformative polytomy a 50% majority rule tree was used, marked by an asterisk. In one case this still resulted in a polytomy. Bold denotes when there are significant differences between the results of the two methods, and in these instances BEAST is always more accurate.

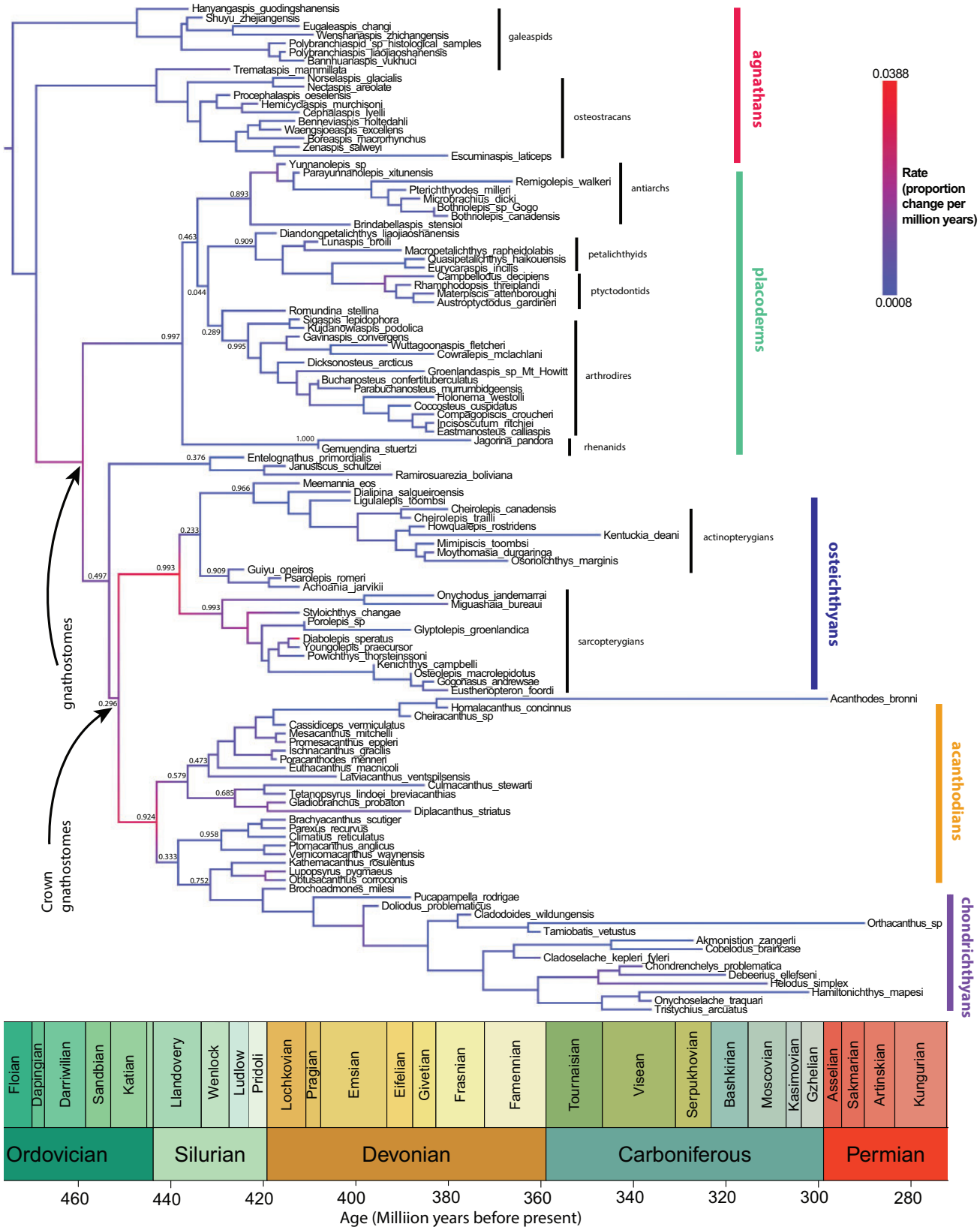

FIGURE 3. Consensus tree from BEAST2. Maximum clade credibility tree with median node heights. Colours refer to evolutionary rates, branch numbers are clade support values (posterior probabilities) for key basal nodes, which often exhibit weak support. This topological uncertainty on basal branches leads to some unusual clades with low support (e.g., *Entelognathus*, *Janusiscus*, *Ramirosuarezia*) appearing in the consensus tree.

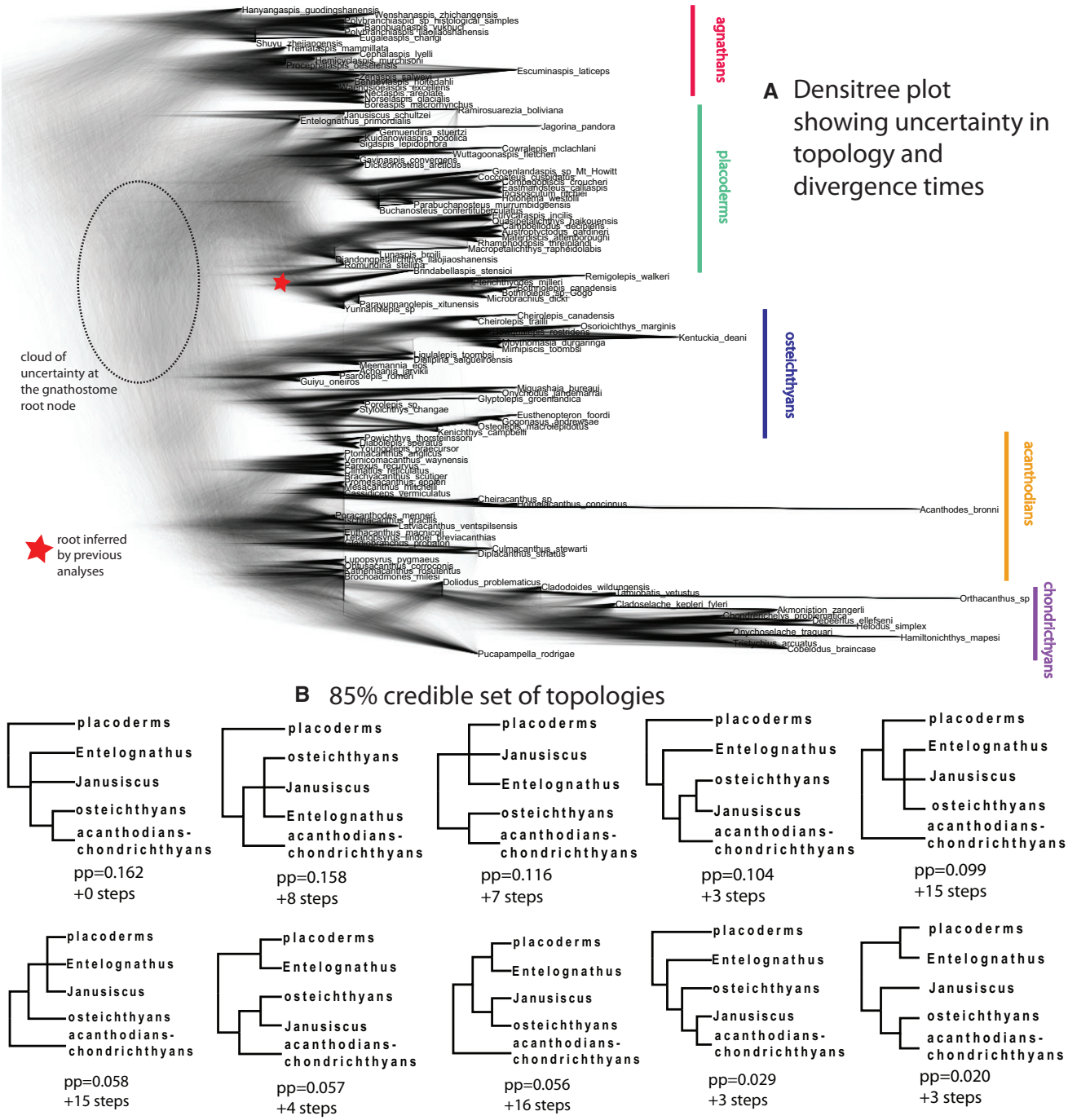

FIGURE 4. Topological uncertainty in the BEAST analysis. **a**) Densitree plot of the posterior sample of trees. **b**) Posterior probabilities of various topologies involving the three major gnathostome groups (placoderms, osteichthyans, and acanthodians–chondrichthyans) along with *Janusiscus* and *Entelognathus*. Posterior probabilities are conditional on placoderms, osteichthyans, and acanthodians–chondrichthyans being monophyletic, and the unstable *Ramirosuarezia* was pruned from all trees prior to calculation. Many of these topologies are contradictory to much morphological evidence, as shown by their parsimony scores.

the number of nodes separating the correct (simulated) root from the inferred root (as found on the consensus tree); 0 means the correct root was found.

Both methods are found to perform significantly better on the balanced tree than the unbalanced tree (likely due to the shorter branch lengths around the root in the unbalanced tree). Parsimony performs badly (root incorrect by 4 or more nodes) in 1 out of 12 of the balanced trees and 8 out of 12 unbalanced trees. The consensus tree from the tip-dated morphological clock analyses

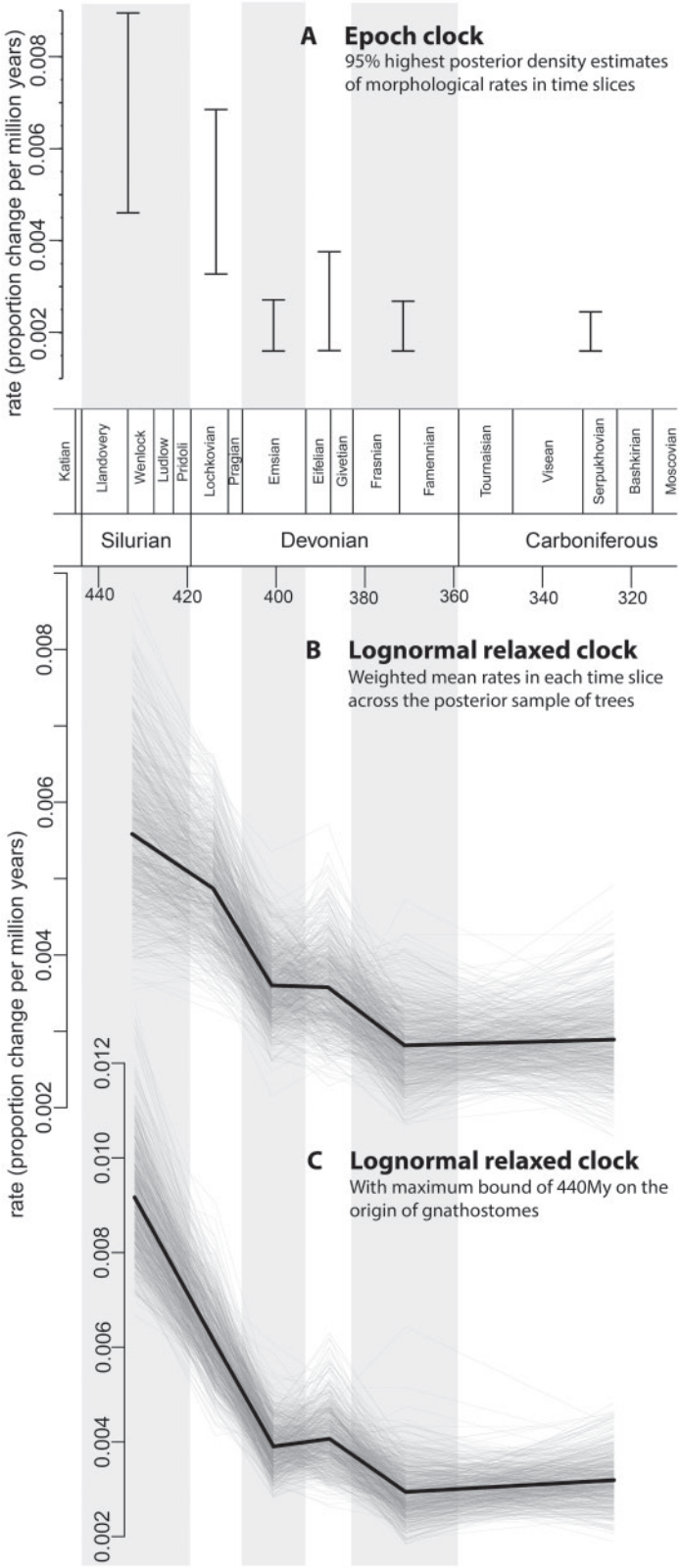

FIGURE 5. Rates of evolution during the Silurian and Devonian. **a**) Epoch clock analysis in Beast 1. 95% HPD intervals for evolutionary rate in each time slice, which correspond to the indicated geological intervals. **b**) Weighted mean rates in each time slice estimated for each tree in the posterior sample from a relaxed clock analysis, with no node age constraints. **c**) Same as b, but with an informative prior on the maximum age of gnathostome divergence at 440 Ma, accentuating the early burst of evolution. The tree samples for b and c were thinned by a factor of 10 before plotting.

performs better, with corresponding frequencies for badly estimated roots being 0 out of 12, and 2 out of 12. As in the analysis of the empirical data set, this analysis shows much uncertainty regarding the root position. Only 2 out of the 24 simulations show strong support for the correct root. However, only a single simulation analysis failed to sample the correct root at appreciable probability, and in this case parsimony found the identical, incorrect tree.

This limited simulation study suggests that when the outgroup is inapplicable (or unknown) for many characters, phylogenetic analysis struggles to root the tree correctly. However, it is notable that when the results from parsimony and the tip-dated clock analysis are very different, the tip-dated clock analysis is always more accurate. At least for data sets similar to this one, this simulation study shows that tip-dated clock methods outperform parsimony in inferring the root position of the tree when traits in the outgroup are not very informative, but neither method performs particularly well. The major caveat of this approach, as for all such simulations, is that the simulation used the same models as BEAST, and therefore the results are only useful if the model realistic at least to some extent. It is notable that the parsimony results appear affected by a high level of long branch attraction in the reanalysis of the simulated data. The tip-dated clock analysis was not affected by this problem, but it complicated the results as parsimony tree was often highly inaccurate in other ways apart from being incorrectly rooted.

Predictable Patterns of Rate Variability in Trees with the Wrong Root

Simulation 1 on the balanced tree has parsimony rooting the ingroup in the wrong position, producing an unbalanced tree similar in shape to an empirical parsimony tree in which placoderms are paraphyletic. This provides potential for comparison of patterns of rate variation between simulated trees known to be incorrectly rooted, and the empirical trees that are suspected to be so (Fig. 6). A tree that is incorrectly rooted on a derived nested taxon artificially temporally compresses the "backbone" of branches between this taxon and the true root (gray branches, Fig. 6a,b). The side branches coming off this backbone would conversely be temporally stretched (black branches, Fig. 6a,b). Rates of evolution along the backbone should therefore be artificially increased, whereas rates on side lineages should be artificially decreased, when the tree has been rooted incorrectly. It is thus possible to characterize a clock "signature" of incorrect rooting, by comparing incorrectly and correctly rooted trees. A Bayesian clock analysis of the data from simulation 1 was run, but this time with the tree constrained to match the (incorrect) results from parsimony (Fig. 6b). Rates along the branches from the root inferred by parsimony were compared with rates along the lineages branching off this backbone. These were compared with rates on the equivalent branches in the correctly rooted trees. In the correctly rooted trees, rates on the (true) backbone and the (true) side lineages showed broadly overlapping distributions around the mean rates inferred for the whole tree. As predicted, in the incorrectly rooted tree, the (incorrectly inferred) backbone branch rates were greatly accelerated, whereas the (incorrectly inferred) side branch rates were decreased (Fig. 6c).

The empirical data from the gnathostome phylogeny show remarkably similar patterns (Fig. 6d). The pattern from the placoderm monophyly tree (Fig. 3) matches the pattern from the correctly rooted tree from the simulations. However, repeating the analysis but constraining the data to one of the shortest parsimony trees implying placoderm paraphyly results in patterns of rate heterogeneity that closely match the simulated incorrectly rooted tree. In fact, the empirical data shows an even stronger pattern: under placoderm paraphyly, there is no overlap at all between the rates on the backbone branches and the side branches, and no overlap of either with the mean rate for the tree.

It is important to note that the tip-dated consensus tree (with placoderm monophyly, Fig. 3) differs from the parsimony tree (with placoderm paraphyly) not just in the position of the gnathostome root, but also in other weakly supported topological details. Therefore, it is possible that the rate heterogeneity seen in the analysis of the second tree is a product topological constraints other than a different gnathostome root. To test this, another analysis was run such that the topologies of the consensus trees were identical aside from the root position, with the precise reverse constraints of the constrained paraphyly analysis (i.e., the placoderm paraphyly tree was rerooted to produce placoderm monophyly). Patterns of rate heterogeneity for this constrained monophyly tree (Supplementary Fig. S4, available on Dryad) were essentially identical to those on the unconstrained placoderm monophyly tree (Fig. 6). This shows that the patterns of rate heterogeneity for the placoderm paraphyly tree are a consequence of paraphyly itself rather than an artefact of constraining topology.

The incorrectly rooted simulated trees, and the empirical trees rerooted with paraphyletic placoderms, show extreme amounts and distinct distributions of rate variation on basal branches, leading to increased among-lineage variability in evolutionary rates. The standard deviation of the lognormal rate distribution in the placoderm paraphyly tree is 1.108, while it is 0.973 in the monophyly tree, although the posterior distributions are overlapping (the 95% HPD intervals are 0.9233–1.2954 for the paraphyly tree and 0.7918–1.1628 for the monophyly tree). The estimated standard deviation in the incorrectly rooted simulation tree is 1.038 (HPD 0.8967–1.1731), compared with 0.942 (HPD 0.8191–1.0818) in the correctly rooted tree.

Although it is possible that the paraphyletic rooting in the empirical tree is correct, and the attendant rate patterns are "simply what happened", the striking resemblance of these patterns to those in known misrooted trees of simulated data suggests that

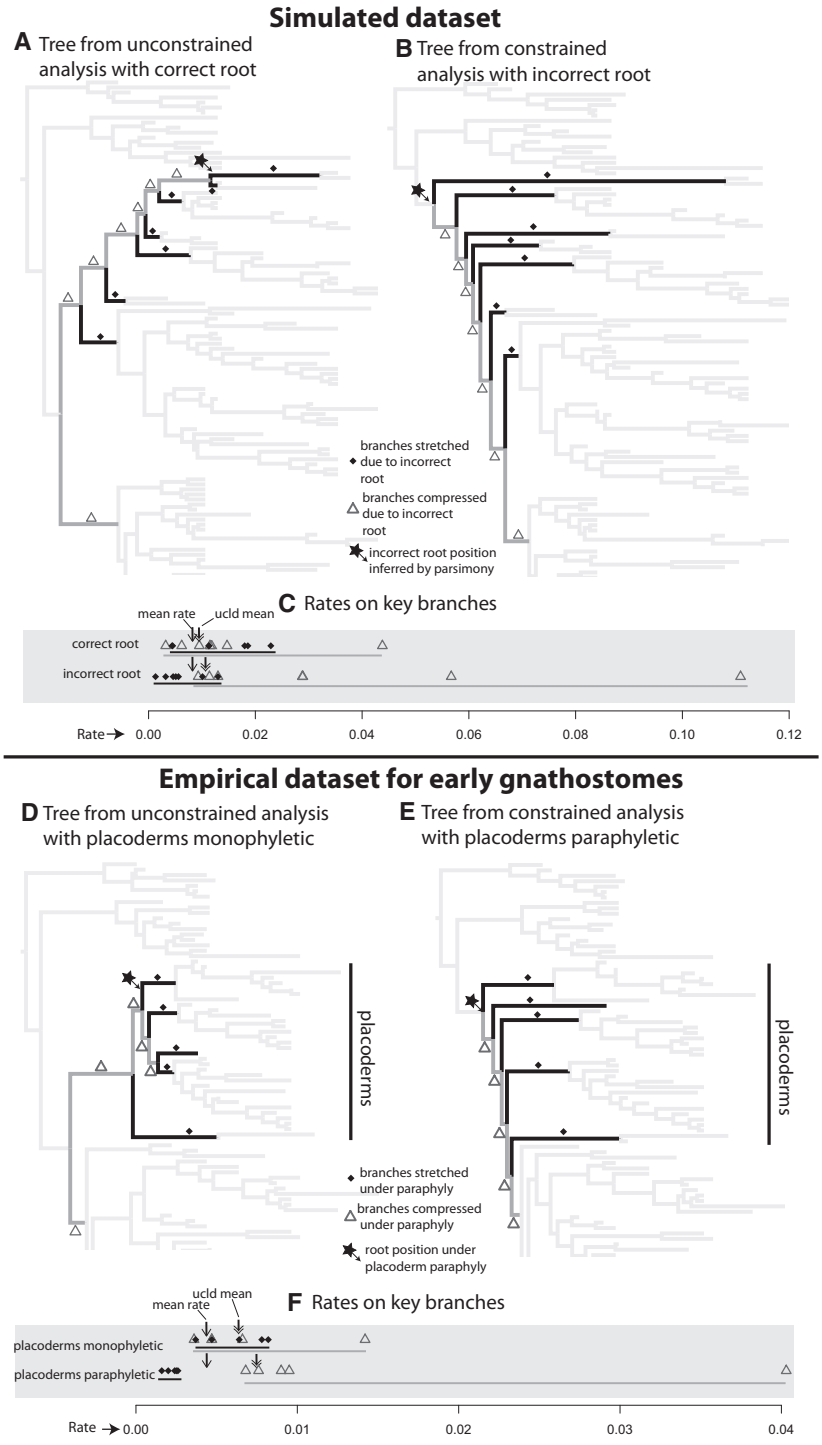

FIGURE 6. Trees known to be incorrectly rooted exhibit distinct patterns of evolutionary rates, similar to those in the empirical trees with placoderm paraphyly. **a–c**) Results for a simulated data set (simulation 1 on tree 1 Table 2). a) Tree from unconstrained tip dating analysis, which retrieved the correct root position. b) Tree from constrained tip dating analysis with incorrect root position (the root position found in parsimony analysis of the same data set). Star indicates the incorrect root. Dark gray branches (triangles) are temporally compressed in the incorrectly rooted tree and black branches (diamonds) temporally lengthened, thus increasing and decreasing evolutionary rates, respectively. c) Branch rates on the trees with the correct root (Fig. 6a) and the incorrect root (Fig. 6b). Branch rates on the lineage between the correct and the incorrect root (Fig. 6a,b, dark gray) are inflated when analyzed with the incorrect root, and side branches (Fig. 6a,b, black) have reduced rates. The ranges of rates on these two sets of branches overlap around the (weighted) mean rate for the whole tree (arrow) in the correctly rooted tree, but are sharply divergent in the incorrectly rooted tree. Similar patterns are found in the empirical gnathostomes data set (**d–f**). d) Unconstained tree, with placoderm monophyly tree, e) Constrained tree, enforcing placoderm paraphyly. Star indicates the root under placoderm paraphyly. Dark gray branches (triangles) would be temporally compressed in the paraphyly tree and black branches (diamonds) temporally lengthened. When placoderms are retrieved as monophyletic, rates for these two sets of branches broadly overlap each other and with weighted mean rate (arrow) for the rest of the tree, but when placoderms are constrained to be paraphyletic, rates for these two sets of branches are sharply divergent.

placoderm paraphyly also represents an incorrect rooting.

Discussion

Topological Effects of using Tip-Dated Clock Methods

Although placoderm paraphyly and monophyly are almost equally parsimonious, the tip-dated morphological clock analysis strongly supports placoderm monophyly over paraphyly. Even after reinstating revised characters so that parsimony supported paraphyly, the tip-dated clock analysis still retrieved strong support for monophyly. Tip-dated clock analysis utilizes a broader range of evolutionary data than other methods, incorporating stratigraphic ages of terminal taxa and estimates of rates of character change. Even if there is little cladistic character information available to choose between alternative topologies, these alternative topologies might still be expected to produce contrasting patterns of rates of evolution, when tip-age data are taken into account. Only a morphological clock analysis would be able to make use of this information directly during topology search. In the early gnathostomes data set, the outgroup taxa are highly derived, and their body plans are so fundamentally different to gnathostomes that they are not particularly useful for polarizing characters. Only about a quarter of characters are scorable to both the outgroup and the ingroup, and some of these are invariant in the ingroup. Thus, the outgroups provide limited power to distinguish between alternative rootings where placoderms are either monophyletic or paraphyletic.

However, placoderm paraphyly apparently requires extremely unbalanced rates of evolution, with the branches leading to each placoderm subgroup exhibiting greatly decreased rates relative to the gnathostome stem lineage (Fig. 6). Simulations suggest that such patterns might be symptomatic of an incorrect rooting, and also suggest that Bayesian tip-dated morphological clock methods outperform parsimony in rooting trees when the outgroup and ingroup shared few applicable characters. The tip-dated clock method is likely to also select trees that are more consistent with stratigraphy: any model that assumes morphological change is (even very roughly) proportional to time will favor a basal position for ancient, plesiomorphic forms, and a nested position for recent, apomorphic forms. The resultant tree with placoderm monophyly indeed suggests a more basal position for very ancient forms such as *Entelognathus* and other Silurian taxa.

It is easy to imagine convergent evolution resulting in parsimony grouping together distantly related taxa that might also be of very different ages. However, morphological clock analyses might reveal that this artifactual topology implies unusual patterns of evolutionary rates and implied stratigraphic ranges. It is notable that major topological differences obtained from using a tip-dated clock analysis have not been previously reported (to our knowledge). Major topological differences appear in this gnathostomes data set, where the derived nature of the outgroup would be expected to cause issues with rooting the tree, and where the typical parsimony result (Brazeau 2009) is known to be controversial (Brazeau and Friedman 2015; Long et al. 2015).

There are however caveats associated with Bayesian tip-dated clock methods. The simulation study necessarily uses the same model as the analysis, so whether or not the superior performance of the Bayesian method is meaningful depends on the ability to the model to replicate the actual process underlying real morphological data. In addition, the tip-dated clock analysis appears to inflate uncertainty near the root of the tree, where topologies can be sampled which are contradictory to a large amount of character evidence. For example, placoderms as sister group to osteichthyans is at least 15 steps longer under parsimony. On the basal branches of the tree where large amounts of character change occurs due to fast evolutionary rates, the Bayesian analysis can accommodate a large amount of homoplasy. Whether these allowed amounts of homoplasy are realistic or not needs to be more fully investigated.

Rates of Evolution, Divergence Time, and Topological Uncertainty

The elevated rates of evolution during the Silurian period retrieved in this analysis suggest that there was a rapid adaptive radiation following the origin of jaws. Our results mirror the findings from measures of lower jaw disparity (Anderson et al. 2011), which showed an increase in disparity into the Early Devonian, and relative stability thereafter.

There is strong information in the ages and morphologies of the fossil terminal taxa (tips) about divergence dates and rates of evolution across the tree. The divergence time for gnathostomes is given as 459 Ma (95% HPD 446.09–473.83) in the focal analysis. This is retrieved without any informative priors (constraints) on the root age of the tree or any internal nodes. This ancient age implies a ghost range of ~35 Myr for gnathostomes. However, fragmentary remains of the putative gnathostome *Skiichthys* (Smith and Sansom 1997) occur at ca. 450 Ma. *Skiichthys* was suggested to have acanthodian or placoderm affinity, that is, nested within gnathostomes. This would imply that the dates retrieved from the Bayesian analysis are not old enough. Mongolepids are a group of putative chondrichthyans that appear in the early Silurian (Karatajute-Talimaa et al. 1990). *Tantalepis* (Sansom et al. 2012) and *Areyonga* (Young 1997) are putative chondrichthyan scale taxa from the Darriwilian (ca. 458–467 Ma) of Australia. A chondrichthyan affinity for these taxa would similarly require the tree to be stretched further back. Nevertheless, these putative crown group gnathostomes are fragmentary and their stratigraphic

age stands in great contrast to the younger ranges of articulated remains.

Similarly, even without any informative root or node age priors, the analysis shows elevated rates of evolution prior to the Devonian. Forcing a younger age for the origin of gnathostomes (bringing age estimates more in line with the ranges of undisputed articulated gnathostome fossils) would compress branches at the base of the tree and thus accentuate this pattern further, as shown in the analysis with a maximum age of 440 My on the gnathostome node. Such "ancient dates or accelerated rates" have been shown for mammals (Beck and Lee 2014). Regardless, gnathostomes were already quite disparate by the late Silurian, and this may be a major cause of the difficulty in determining the tree topology during this period. The inability of morphological data alone to resolve relationships among even well-known living vertebrates is well known (e.g., Reeder et al. 2015), and similar problems should be expected in early gnathostomes.

Convergent Evolution in Morphological Data Sets, and Basal Benthic Placoderms

Convergent evolution is well known to be a major cause of problems in morphological data sets, and it is common for groups with similar ecologies to be incorrectly grouped together, as exemplified by legless lizards and snakes (Lee 1998; Reeder et al. 2015). It is notable therefore that both outgroups and the most basal placoderm taxa (under the paraphyly hypothesis) are presumably benthic species. Adaptation to a benthic niche might be expected to lead to convergent adaptations that could be (mis)interpreted as homologous plesiomorphies shared by the outgroup and certain placoderms. Such traits include a dorsal migration of the orbits and nares and a concomitant anterior migration of the jaws. Three of the four characters supporting paraphyly can be linked to these changes, most obviously the characters involving the dorsal position of the orbits and nares. The contact of the pineal plate with the orbits is also likely to be linked with migration of the orbits toward the midline. Since the nasal capsules are part of an independent endocranial unit in placoderms (one of the characters supporting placoderm monophyly), this likely had a profound effect on the development of placoderm braincases, possibly increasing the degree to which the nasal capsules could move relative to other sense organs. The possibility that morphological clock methods, through consideration of additional sources of information such as stratigraphy and evolutionary rates, can better identify and accommodate morphological convergence may be a productive area for future study.

Implications of Placoderm Monophyly versus Paraphyly

The hypotheses of placoderm monophyly and paraphyly offer starkly contrasting frameworks with important ramifications for the understanding key events in early vertebrate evolution. Under placoderm paraphyly, shared features of placoderms are presumed to be primitive and thus ancestral for all gnathostomes, whereas under placoderm monophyly, these features become unique specializations of placoderms alone. The evolution of jaw bones was previously assumed to start with the simple jaws of placoderms, with a single dermal lower jaw bone and no upper jaw (maxilla). Dermal jaw bones were then added near the crown gnathostome node with the appearance of a maxilla, dentary, infradentaries, and gulars. Under placoderm monophyly, this scenario can no longer be assumed to be correct. The position of *Entelognathus* is key, and it is retrieved as sister group to placoderms fairly often in the Bayesian analysis. If this is correct then it would mean that osteichthyan-like jaw bones could be the ancestral condition for jawed vertebrates. Jaws may have first evolved with a complex covering of dermal bones which was later reduced to a single lower jawbone and palatal toothplates in placoderms.

Placoderms might therefore be viewed as highly specialized dead end, rather than the ground plan for all other gnathostomes. In particular, the presence of a unique set of claspers and internal fertilization are potential placoderm synapomorphies likely profoundly affecting their biology. Another consequence of placoderm monophyly would be a significant decrease in the number of nodes in the phylogeny between the origin of jaws and the common ancestor of crown gnathostomes. Placoderm paraphyly results in a highly asymmetrical tree where basal gnathostomes are all placoderms, but placoderm monophyly has a more balanced tree where placoderms, *Entelognathus,* osteichthyans, and chondrichthyans could be considered almost equally "basal" (Fig. 4b). Thus, the ancestral condition for gnathostomes becomes much more uncertain, with the major groups of placoderms, acanthodians, and osteichthyans already diversified by the late Silurian. The rates analysis is consistent with this scenario, with fast morphological rates and long ghost lineages being found at the base of the tree.

Supplementary Material

Data available from the Dryad Digital Repository: http://dx.doi.org/10.5061/dryad.v30f1.

Funding

This work was supported by the Australian Research Council (to J.A.L.).

Acknowledgements

Mike Coates, Vincent Dupret, Per Ahlberg, Jing Lu, You'an Zhu, Brian Choo, Zerina Johanson, and Alice Clement are thanked for discussions on early vertebrate morphology, and Nick Matzke for discussions about tip-dating. Alexandra Gavryushkina and Guy Baele

answered questions via the BEAST google group. Martin Brazeau provided helpful comments on the manuscript, and we thank Thomas Near as editor.

References

Anderson P.S., Friedman M., Brazeau M.D., Rayfield E.J. 2011. Initial radiation of jaws demonstrated stability despite faunal and environmental change. Nature 476:206–209.

Baele G., Lemey P., Bedford T., Rambaut A., Suchard M.A., Alekseyenko A.V. 2012. Improving the accuracy of demographic and molecular clock model comparison while accommodating phylogenetic uncertainty. Mol. Biol. Evol. 29:2157–2167.

Beck R.M., Lee M.S. 2014. Ancient dates or accelerated rates? Morphological clocks and the antiquity of placental mammals. Proc. R. Soc. B 281:20141278.

Bell M. 2015. geoscale: geological time scale plotting. R package version 2.0. Available from: URL https://CRAN.R-project.org/package=geoscale.

Bielejec F., Lemey P., Baele G., Rambaut A., Suchard M.A. 2014. Inferring heterogeneous evolutionary processes through time: from sequence substitution to phylogeography. Syst. Biol. 63:493–504.

Blackburn D.G. 2015. Evolution of vertebrate viviparity and specializations for fetal nutrition: a quantitative and qualitative analysis. J. Morphol. 276:961–990.

Bouckaert R., Heled J., Kühnert D., Vaughan T., Wu C.-H., Xie D., Suchard M.A., Rambaut A., Drummond A.J. 2014. BEAST 2: a software platform for Bayesian evolutionary analysis. PLoS Comput. Biol. 10:e1003537.

Bouckaert R.R. 2010. DensiTree: making sense of sets of phylogenetic trees. Bioinformatics 26:1372–1373.

Brazeau M.D. 2009. The braincase and jaws of a Devonian 'acanthodian' and modern gnathostome origins. Nature 457:305–308.

Brazeau M.D., de Winter V. 2015. The hyoid arch and braincase anatomy of *Acanthodes* support chondrichthyan affinity of 'acanthodians'. Proc. R. Soc. B 282:20152210.

Brazeau M.D., Friedman M. 2014. The characters of Palaeozoic jawed vertebrates. Zool. J. Linn. Soc. 170:779–821.

Brazeau M.D., Friedman M. 2015. The origin and early phylogenetic history of jawed vertebrates. Nature 520:490–497.

Carr R.K., Hlavin W.J. 2010. Two new species of *Dunkleosteus* Lehman, 1956, from the Ohio Shale Formation (USA, Famennian) and the Kettle Point Formation (Canada, Upper Devonian), and a cladistic analysis of the Eubrachythoraci (Placodermi, Arthrodira). Zool. J. Linn. Soc. 159:195–222.

Close R.A., Friedman M., Lloyd G.T., Benson R.B. 2015. Evidence for a mid-Jurassic adaptive radiation in mammals. Curr. Biol. 25: 2137–2142.

Coates M., Sequeira S. 2001. A new stethacanthid chondrichthyan from the Lower Carboniferous of Bearsden, Scotland. J. Vertebr. Paleontol. 21:438–459.

Davis S.P., Finarelli J.A., Coates M.I. 2012. *Acanthodes* and shark-like conditions in the last common ancestor of modern gnathostomes. Nature 486:247–250.

Drummond A.J., Ho S.Y., Phillips M.J., Rambaut A. 2006. Relaxed phylogenetics and dating with confidence. PLoS Biol. 4:e88.

Drummond A.J., Suchard M.A., Xie D., Rambaut A. 2012. Bayesian phylogenetics with BEAUti and the BEAST 1.7. Mol. Biol. Evol. 29:1969–1973.

Dupret V. 2010. Revision of the genus *Kujdanowiaspis* Stensiö, 1942 (Placodermi, Arthrodira,"Actinolepida") from the Lower Devonian of Podolia (Ukraine). Geodiversitas 32:5–63.

Dupret V., Sanchez S., Goujet D., Tafforeau P., Ahlberg P.E. 2014. A primitive placoderm sheds light on the origin of the jawed vertebrate face. Nature 507:500–503.

Dupret V., Zhu M., Wang J.Q. 2009. The morphology of *Yujiangolepis liujingensis* (Placodermi, Arthrodira) from the Pragian of Guangxi (South China) and its phylogenetic significance. Zool. J. Linn. Soc. 157:70–82.

Forey P. 1980. *Latimeria*: a paradoxical fish. Proc. R. Soc. B 208:369–384.

Friedman M. 2007. *Styloichthys* as the oldest coelacanth: implications for early osteichthyan interrelationships. J. Syst. Palaeontol. 5: 289–343.

Gai Z., Donoghue P.C., Zhu M., Janvier P., Stampanoni M. 2011. Fossil jawless fish from China foreshadows early jawed vertebrate anatomy. Nature 476:324–327.

Gardiner B.G. 1984a. The relationship of placoderms. J. Vertebr. Paleontol. 4:379–395.

Gardiner B.G. 1984b. The relationships of the paleoniscid fishes. A review based on new specimens of *Mimia* and *Moythomasia* from the upper Devonian of Western Australia. Bull. Br. Mus. (Nat. Hist.) Geol. 37:173–248.

Gavryushkina A., Heath T.A., Ksepka D.T., Stadler T., Welch D., Drummond A.J. 2015. Bayesian total evidence dating reveals the recent crown radiation of penguins. arXiv preprint arXiv:1506.04797.

Gavryushkina A., Welch D., Stadler T., Drummond A.J. 2014. Bayesian inference of sampled ancestor trees for epidemiology and fossil calibration. PLoS Comput. Biol. 10:e1003919.

Giles S., Friedman M., Brazeau M.D. 2015. Osteichthyan-like cranial conditions in an Early Devonian stem gnathostome. Nature 520: 82–85.

Goloboff P.A., Farris J.S., Nixon K.C. 2008. TNT, a free program for phylogenetic analysis. Cladistics 24:774–786.

Goodrich E.S. 1930. Studies on the structure and development of vertebrates. London: Macmillan.

Goujet D. 1982. Les affinités des placodermes, une revue des hypothèses actuelles. Geobios 15:27–38.

Goujet D. 1984a. Les poissons placodermes du Spitzberg: Arthrodires Dolichothoraci de la Formation de Wood Bay (Dévonien inférieur). Cahiers de Paléontologie, Section Vertebrés. CNRS, Paris.

Goujet D. 1984b. Placoderm interrelationships: a new interpretation, with a short review of placoderm classifications. Proceedings of The Linnean Society of New South Wales. p. 211–243.

Goujet D. 2001. Placoderms and basal gnathostome apomorphies. In: Ahlberg P.E., editor. Major events in early vertebrate evolution. London and New York: Taylor and Francis. p. 209–222.

Goujet D., Young G.C. 2004. Placoderm anatomy and phylogeny: new insights. In: Arratia G., Wilson M.V.H., Cloutier R., editors. Recent advances in the origin and early radiation of vertebrates. München: Verlag Dr. Friedrich Pfeil. p. 109–126.

Janvier P. 1985. Les Céphalaspides du Spitsberg. Anatomie, phylogénie et systématique des Ostéostracés siluro-dévoniens. Révision des Ostéostracés de la formation de Wood Bay (Dévonien inférieur du Spitsberg). Cahiers de Paléontologie, Section Vertebrés. CNRS, Paris.

Janvier P. 1996. Early vertebrates. Oxford: Clarendon Press.

Jarvik E. 1980. Basic structure and evolution of vertebrates. London: Academic Press.

Jia L.-T., Zhu M., Zhao W.-J. 2010. A new antiarch fish from the Upper Devonian Zhongning Formation of Ningxia, China. Palaeoworld 19:136–145.

Johanson Z. 2002. Vascularization of the osteostracan and antiarch (Placodermi) pectoral fin: similarities, and implications for placoderm relationships. Lethaia 35:169–186.

Johnston J.B. 1905. The cranial nerve components of *Petromyzon*. Gegenbaurs Morphol. Jahrb. 34:149–203.

Jombart T., Aanensen D.M., Baguelin M., Birrell P., Cauchemez S., Camacho A., Colijn C., Collins C., Cori A., Didelot X. 2014. OutbreakTools: a new platform for disease outbreak analysis using the R software. Epidemics 7:28–34.

Karatajute-Talimaa V., Novitskaya L., Rozman K., Sodov Z. 1990. *Mongolepis*—a new lower Silurian genus of elasmobranchs from Mongolia. Paleontol. Zh. 1990:76–86.

Kembel S.W., Cowan P.D., Helmus M.R., Cornwell W.K., Morlon H., Ackerly D.D., Blomberg S.P., Webb C.O. 2010. Picante: R tools for integrating phylogenies and ecology. Bioinformatics 26:1463–1464.

Kuratani S., Ueki T., Aizawa S., Hirano S. 1997. Peripheral development of cranial nerves in a cyclostome, *Lampetra japonica*: morphological distribution of nerve branches and the vertebrate body plan. J. Comp. Neurol. 384:483–500.

Lee M.S.Y. 1998. Convergent evolution and character correlation in burrowing reptiles: towards a resolution of squamate relationships. Biol. J. Linn. Soc. 65:369-453.

Lee M.S.Y., Cau A., Naish D., Dyke G.J. 2014. Morphological clocks in paleontology, and a mid-Cretaceous origin of crown Aves. Syst. Biol. 63:442–449.
Long J.A., Mark-Kurik E., Johanson Z., Lee M.S., Young G.C., Min Z., Ahlberg P.E., Newman M., Jones R., Den Blaauwen J. 2015. Copulation in antiarch placoderms and the origin of gnathostome internal fertilization. Nature 517:196–199.
Lu J., Zhu M., Long J.A., Zhao W., Senden T.J., Jia L., Qiao T. 2012. The earliest known stem-tetrapod from the Lower Devonian of China. Nat. Commun. 3:1160.
Maddison W.P., Maddison D.R. 2015. Mesquite: a modular system for evolutionary analysis. Version 3.04. Available from: URL http://mesquiteproject.org.
Maisey J.G. 2005. Braincase of the Upper Devonian shark *Cladodoides wildungensis* (Chondrichthyes, Elasmobranchii), with observations on the braincase in early chondrichthyans. Bull. Am. Mus. Nat. Hist. 288:1–103.
Matzke N.J. 2015. BEASTmasteR: R tools for automated conversion of NEXUS data to BEAST2 XML format, for fossil tip-dating and other uses. Instructions at PhyloWiki. Available from: URL http://phylo.wikidot.com/beastmaster.
Miles R.S., Young G.C. 1977. Placoderm interrelationships reconsidered in the light of new ptyctodontids from Gogo, Western Australia. Linn. Soc. Symp. Ser. 4:123–198.
Miller M.A., Pfeiffer W., Schwartz T. 2010. Creating the CIPRES Science Gateway for inference of large phylogenetic trees. Gateway Computing Environments Workshop (GCE); 2010; IEEE. p. 1–8.
Miyashita T. 2015. Fishing for jaws in early vertebrate evolution: a new hypothesis of mandibular confinement. Biol. Rev. 91:611–657.
Orme D., Freckleton R., Thomas G., Petzoldt T., Fritz S., Isaac N., Pearse W. 2013. caper: comparative analysis of phylogenetics and evolution in R. R package version 0.5.2. Available from: URL https://CRAN.R-project.org/package=caper.
Ørvig T. 1962. Y at-il une relation directe entre les arthrodires ptyctodontides et les holocephales. Colloq. Int. CNRS 104:49–61.
Pan Z., Zhu M., Zhu Y.A., Jia L. 2015. A new petalichthyid placoderm from the Early Devonian of Yunnan, China. C. R. Palevol. 14:125–137.
Paradis E., Claude J., Strimmer K. 2004. APE: analyses of phylogenetics and evolution in R language. Bioinformatics 20:289–290.
Pradel A., Maisey J.G., Tafforeau P., Janvier P. 2009. An enigmatic gnathostome vertebrate skull from the Middle Devonian of Bolivia. Acta Zool. 90:123–133.
Pradel A., Tafforeau P., Maisey J.G., Janvier P. 2011. A new Paleozoic Symmoriiformes (chondrichthyes) from the Late Carboniferous of Kansas (USA) and cladistic analysis of early chondrichthyans. PLoS One 6:e24938.
Rambaut A., Suchard M.A., Xie D., Drummond A.J. 2014. Tracer v1.6. Available from: URL http://beast.bio.ed.ac.uk/Tracer.
Reeder T.W., Townsend T.M., Mulcahy D.G., Noonan B.P., Wood P.L. Jr, Sites J.W. Jr, Wiens J.J. 2015. Integrated analyses resolve conflicts over squamate reptile phylogeny and reveal unexpected placements for fossil taxa. PLoS One 10:e0118199.
Rücklin M., Donoghue P.C., Johanson Z., Trinajstic K., Marone F., Stampanoni M. 2012. Development of teeth and jaws in the earliest jawed vertebrates. Nature 491:748–751.
Sansom I.J., Davies N.S., Coates M.I., Nicoll R.S., Ritchie A. 2012. Chondrichthyan-like scales from the Middle Ordovician of Australia. Palaeontology 55:243–247.
Sansom R.S. 2009. Phylogeny, classification and character polarity of the Osteostraci (Vertebrata). J. Syst. Palaeontol. 7:95–115.
Schaeffer B. 1971. The braincase of the holostean fish *Macrepistius*, with comments on neurocranial ossification in the Actinopterygii. American Museum of Natural History.
Schaeffer B. 1975. Comments on the origin and basic radiation of the gnathostome fishes with particular reference to the feeding mechanism. Colloq. Int. CNRS 218:101–109.
Smith M.M., Johanson Z. 2003. Separate evolutionary origins of teeth from evidence in fossil jawed vertebrates. Science 299:1235–1236.
Smith M.M., Sansom I.J. 1997. Exoskeletal micro-remains of an Ordovician fish from the Harding Sandstone of Colorado. Palaeontology 40:645–658.
Stadler T. 2010. Sampling-through-time in birth–death trees. J. Theor. Biol. 267:396–404.
Stensiö E.A. 1927. The Downtonian and Devonian vertebrates of Spitsbergen. I, Family Cephalaspidae. Skrifter om Svalbard og Ishavet 12:1–391.
Stensiö E.A. 1963. Anatomical studies on the arthrodiran head. Stockholm: Almqvist & Wiksell.
Stensiö E.A. 1969. Elasmobranchiomorphi Placodermata Arthrodires. In: Piveteau J., editor. Traité de paléontologie. Paris: Masson. p. 71–692.
Swartz B.A. 2009. Devonian actinopterygian phylogeny and evolution based on a redescription of *Stegotrachelus finlayi*. Zool. J. Linn. Soc. 156:750–784.
Swofford D. 2002. PAUP 4.0 b10: phylogenetic analysis using parsimony. Sunderland (MA): Sinauer Associates.
Trinajstic K., Boisvert C., Long J., Maksimenko A., Johanson Z. 2015. Pelvic and reproductive structures in placoderms (stem gnathostomes). Biol. Rev. Camb. Philos. Soc. 90:467–501.
Trinajstic K., Long J.A. 2009. A new genus and species of Ptyctodont (Placodermi) from the Late Devonian Gneudna Formation, Western Australia, and an analysis of Ptyctodont phylogeny. Geol. Mag. 146:743–760.
Wang N.-Z., Donoghue P.C., Smith M.M., Sansom I.J. 2005. Histology of the galeaspid dermoskeleton and endoskeleton, and the origin and early evolution of the vertebrate cranial endoskeleton. J. Vertebr. Paleontol. 25:745–756.
Young G. 1986. The relationships of placoderm fishes. Zool. J. Linn. Soc. 88:1–57.
Young G.C. 1980. A new Early Devonian placoderm from New South Wales, Australia, with a discussion of placoderm phylogeny. Palaeontogr. Abt. A Palaeozool-Stratigr. 167:10–76.
Young G.C. 1997. Ordovician microvertebrate remains from the Amadeus Basin, central Australia. J. Vertebr. Paleontol. 17:1–25.
Young G.C. 2008. The relationships of antiarchs (Devonian placoderm fishes)—evidence supporting placoderm monophyly. J. Vertebr. Paleontol. 28:626–636.
Young G.C. 2010. Placoderms (armored fish): dominant vertebrates of the Devonian period. Annu. Rev. Earth Planet. Sci. 38:523–550.
Zhu M., Gai Z. 2007. Phylogenetic relationships of galeaspids (Agnatha). Front. Biol. China 2:151–169.
Zhu M., Yu X., Ahlberg P.E., Choo B., Lu J., Qiao T., Qu Q., Zhao W., Jia L., Blom H., Zhu Y.-A. 2013. A Silurian placoderm with osteichthyan-like marginal jaw bones. Nature 502:188–193.
Zhu Y.A., Zhu M., Wang J.Q. 2015. Redescription of *Yinostius major* (Arthrodira: Heterostiidae) from the Lower Devonian of China, and the interrelationships of Brachythoraci. Zool. J. Linn. Soc.